International Journal of Engineering Research

Sirte University
Faculty of Engineering

Journal homepage: Scientific Journals (su.edu.ly)

Effect of Regeneration on the sensitivity of Gas Turbine Performance to Ambient Temperature

Ali Alshommaki[1], Tariq Aboalhol[1]

Libyan authority for scientific research (LASR), The Libyan Higher Technical Centre for Training and Production, Tripoli, Libya

Corresponding Author: ali.shommaki@tpc.ly & shommalkiali@gmail.com

ARTICLE INFOR

Article history:

Received 12 August 2026

Revised 02 Sept. 2026

Accepted 19 Sept. 2026
Available online

01 November 2026

ABSTRACT

This study evaluates the potential of regenerative heat recovery to mitigate the efficiency and fuel-consumption penalties associated with high ambient temperatures in a GT13DM gas turbine operating at the Southern Tripoli Power Plant in Libya. Steady-state thermodynamic models of simple and regenerative Brayton cycles were developed in Engineering Equation Solver (EES) utilizing temperature-dependent properties, realistic component irreversibilities, and industrial pressure-loss assumptions. The analysis quantifies the influence of seasonal climatic variations and regenerator effectiveness on net power output, thermal efficiency, and specific fuel consumption. Annualized performance assessments weighted by local meteorological occurrence frequencies reveal that elevated ambient temperatures reduce net power output by 18.54% between the winter reference condition (16.21 °C) and the summer extreme condition (39.40 °C), regeneration significantly improves thermal efficiency and fuel utilization. The regenerative configuration increased annualized thermal efficiency by 3.82 percentage points (13.55% relative improvement) and reduced specific fuel consumption by 11.95%. Furthermore, the retrofit reduces annual fuel consumption by approximately 27.51 million kg and CO_2 emissions by approximately 75,381 tons. These findings support the thermodynamic feasibility of integrating regenerators into existing gas turbine infrastructure in hot-climate regions.

2026 Sirte University, All rights reserved

Keywords: *Gas turbine performance; Regenerative Brayton cycle; Ambient temperature derating; Energy efficiency; CO_2 emission reduction.*

1. Introduction

Libya's energy sector has increasingly shifted toward gas turbine power generation [1], reflecting the country's abundant natural gas reserves [2] and growing demand for flexible, fast-response electricity generation systems capable of accommodating fluctuations in power demand [1,3]. Gas turbines are highly attractive for power generation due to their relatively short construction times, operational flexibility, and suitability for meeting peak electrical loads. Consequently, Libya's dependence on gas turbines has increased substantially over the past two decades. Natural gas use for electricity generation increased substantially between 2000 and 2022, while total national electricity production increased by approximately 127% [1].

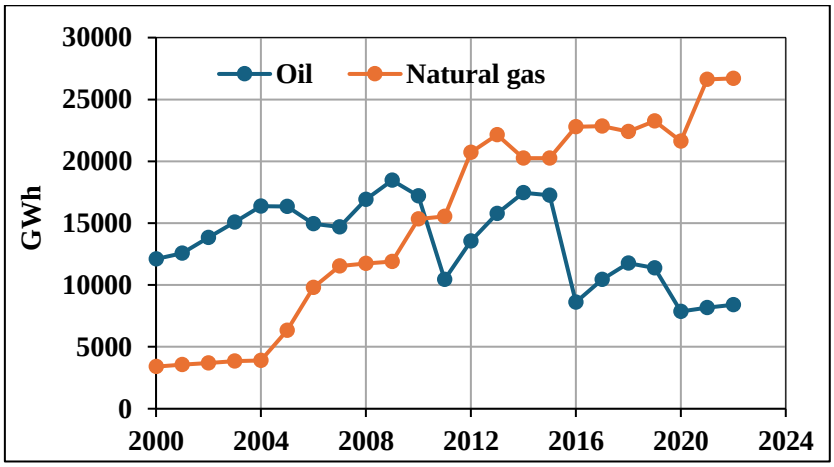


Figure 1. Annual Electricity Generation by Source in Libya (2000-2022)

Despite these advantages, gas turbine performance is highly susceptible to environmental operating conditions, particularly ambient temperature. During continuous base-load operation, the relatively low thermal efficiency of conventional simple gas turbine (SGT) systems results in high fuel consumption and operating costs [6]. In hot climates, elevated ambient temperatures reduce intake-air density and consequently restrict the mass flow rate entering the compressor. This aerothermal derating produces a "turbomachinery scissor effect," in which compressor work increases while gross turbine output decreases, resulting in reductions in both net power output and thermal efficiency [5]. These challenges are particularly acute in Libya, where fuel transportation costs and infrastructure limitations place additional pressure on the electricity system [7]. Furthermore, limited investment in steam-cycle infrastructure has constrained the deployment of

combined-cycle power plants, leaving the electricity system reliant on less efficient SGTs [8].

Among the available gas-turbine performance-enhancement strategies, regeneration has received considerable attention. By recovering thermal energy from turbine exhaust gases to preheat the compressed air before combustion, regenerative gas turbine (RGT) systems reduce the fuel required to achieve the prescribed turbine inlet temperature (TIT) [10,11]. While previous investigations have demonstrated the thermodynamic benefits of regeneration [9–11], limited attention has been given to evaluating RGT operation under representative North African climatic conditions using the operating parameters of existing power-generation assets. Specifically, few studies have translated discrete ambient-temperature variations into annualized, meteorologically weighted performance metrics for an existing Libyan facility.

To bridge this gap, this study investigates the Southern Tripoli Power Plant, utilizing its GT13DM gas turbine as a representative baseline. We hypothesize that retrofitting the existing GT13DM with a regenerator can mitigate the thermal-efficiency penalties associated with ambient-temperature derating while providing annual fuel and carbon-emission savings without the major capital investment required for combined-cycle infrastructure.

Guided by this hypothesis, this study addresses the following core research questions: (1) how does ambient temperature affect aerothermal derating and the thermodynamic state variables of the GT13DM? (2) What are the comparative thermodynamic advantages of the RGT over the SGT across the seasonal temperature range? (3) How sensitive is cycle performance to variations in regenerator effectiveness? (4) What are the annualized fuel, efficiency, and environmental benefits when evaluated against the meteorological profile of Southern Tripoli?

To answer these questions, the primary objectives of this research are to:

1. Develop and validate steady-state thermodynamic models of SGT and RGT configurations using EES.
2. Quantify the influence of ambient temperature on inlet-air density, mass flow rate, power output, and specific fuel consumption.
3. Evaluate the sensitivity of cycle performance to practical ranges of regenerator effectiveness.
4. Determine annualized performance metrics using a temperature-bin weighting methodology based on local climatic data.

5. Assess the environmental implications of regeneration through comparative analysis of CO_2 emissions and qualitative indicators of NOx and CO formation tendencies.

2. Methodology

This study investigates the thermodynamic performance of the GT13DM industrial gas turbine under representative operating conditions at the Southern Tripoli Power Plant. A comparative steady-state thermodynamic modeling approach was adopted, evaluating a baseline simple gas turbine (SGT) cycle against a regenerative gas turbine (RGT) configuration. Both models were developed in Engineering Equation Solver (EES).

The analysis utilizes a pseudo-ideal gas Brayton-cycle framework with variable specific heats. To maintain thermodynamic consistency across the compressor, combustor, regenerator, and turbine sections, the working fluid was modeled as a single pseudo-fluid. The influence of combustion at elevated temperatures was captured using temperature-dependent effective thermodynamic properties obtained from EES built-in property functions, supplemented by polynomial specific-heat correlations for the high-temperature working fluid.

2.1. Simple Gas Turbine Modeling Framework

The SGT configuration consists of four principal thermodynamic states: compressor inlet (1), compressor outlet (2), turbine inlet (3), and turbine outlet (4).

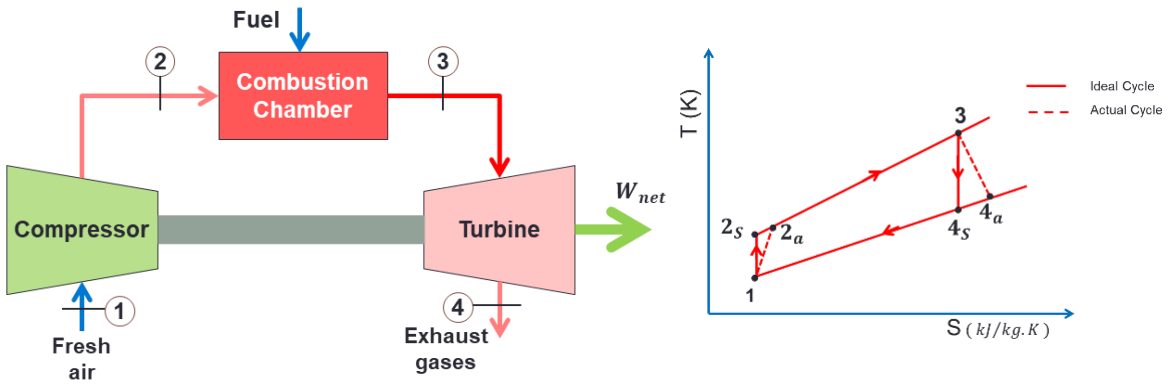


Figure 2. Schematic of the simple gas turbine cycle

Compression and expansion processes were modeled using entropy-based isentropic reference states to evaluate non-isentropic component behavior while accounting for variable thermodynamic properties. Pressure losses in the intake, combustion chamber, and exhaust sections were modeled as fixed fractional pressure drops based on published industrial gas turbine data [18,19].

Non-Isentropic Compression Process (1–2)

Ambient air enters the compressor at temperature $T_1$and pressure P_1. The compressor inlet pressure accounts for a 2% intake pressure loss relative to ambient

atmospheric conditions (P_{amb}):

$$P_1 = P_{amb}(1 - 0.02) \qquad (1)$$

The compressor outlet pressure is determined by the compressor pressure ratio (r_p):

$$P_2 = r_p P_1 \qquad (2)$$

The compression process is modeled using an isentropic reference state. The inlet entropy (s_1) and enthalpy (h_1) are obtained from EES property functions. The isentropic outlet temperature (T_{2s}) is evaluated from the constant-entropy condition $s(T_{2s}, P_2) = s_1$, yielding the isentropic enthalpy h_{2s}. The actual compressor outlet enthalpy (h_2) and temperature (T_2) are then calculated using the compressor isentropic efficiency (η_c):

$$h_2 = h_1 + \frac{h_{2s} - h_1}{\eta_c}, T_2 = T(h_2) \qquad (3)$$

To capture the aerothermal derating caused by ambient temperature variations, the air mass flow rate ($\dot{m}_a$) is not assumed constant. Instead, it is determined from the prescribed compressor volumetric flow rate ($\dot{V}$) and the ambient-air density corresponding to the specified ambient pressure and inlet-air temperature. The ambient pressure is retained in this mass-flow calculation, while the 2% intake pressure loss is applied separately in defining the thermodynamic compressor-inlet state in Eq. (1):

$$\rho_a = \frac{P_1 \times 1000}{R_{air}(T_1 + 273.15)} \ , \quad \dot{m}_a = \rho_a \dot{V} \qquad (4)$$

where P_1 is the compressor inlet pressure, $T_1 = T_a$ is the compressor inlet temperature, R_{air} is the specific gas constant of air, and $\dot{V}$is the prescribed compressor volumetric flow rate.

The compressor power consumption is calculated as:

$$\dot{W}_{comp} = \dot{m}_a(h_2 - h_1) \qquad (5)$$

Constant-Pressure Heat Addition Process (2–3)

Heat addition occurs in the combustion chamber with a fixed fractional pressure drop of 4%:

$$P_3 = P_2(1 - 0.04) \qquad (6)$$

Temperature-dependent air properties were evaluated using EES built-in thermodynamic property functions. The turbine working fluid was represented using the EES Air property model.

$$h_3 = h_{air}(T_3) \, , \qquad s_3 = s_{air}(T_3, P_3) \qquad (7)$$

The fuel mass flow rate ($\dot{m}_f$) is determined from a steady-flow combustor energy balance, accounting for the fuel delivery temperature ($T_f = T_1 = T_a$) and the enthalpy of methane (h_f):

$$\dot{m}_f = \frac{\dot{m}_a(h_3 - h_2)}{\eta_{comb} \times LHV_{HC_4} - (h_3 - h_f)} \qquad (8)$$

The total thermal energy input to the cycle is

$$\dot{Q}_{in} = \dot{m}_f \times LHV_{HC_4} \times \eta_{comb} \qquad (9)$$

Non-Isentropic Expansion Process (3–4)

The turbine exit pressure remains slightly above ambient pressure to overcome a 3% exhaust-duct flow resistance:

$$P_4 = \frac{P_{amb}}{1 - 0.03} \qquad (10)$$

Using the turbine inlet entropy $s_3 = s(T_3, P_3)$, the isentropic outlet temperature (T_{4s}) is determined. The actual turbine outlet temperature (T_4) is calculated using the turbine isentropic efficiency (η_t):

$$T_4 = T(h_3 - \eta_t(h_3 - h_{4s})) \qquad (11)$$

The total working-fluid mass flow through the turbine is

$$\dot{m}_g = \dot{m}_a + \dot{m}_f \qquad (12)$$

The turbine work output ($\dot{W}_{turb}$), net cycle power output ($\dot{W}_{net}$), thermal efficiency (η_{th}), and specific fuel consumption (SFC) are evaluated as follows:

$$\dot{W}_{turb} = \dot{m}_g(h_3 - h_4) \qquad (13)$$

$$\dot{W}_{net} = \dot{W}_{turb} - \dot{W}_{comp} \qquad (14)$$

$$\eta_{th} = \frac{\dot{W}_{net}}{\dot{Q}_{in}}, \qquad SFC = \frac{3600 \times \dot{m}_f}{\dot{W}_{net}} \qquad (15)$$

2.2. Regeneration System Integration

To form the RGT model, a steady-state counterflow regenerator is incorporated between the compressor outlet and the combustion chamber. The regenerator recovers thermal energy from the turbine exhaust (state 4 to 6) to preheat the compressed air (state 2 to 5) as shown in Figures 3 and 4. Heat losses to the surroundings and transient thermal-storage effects are neglected.

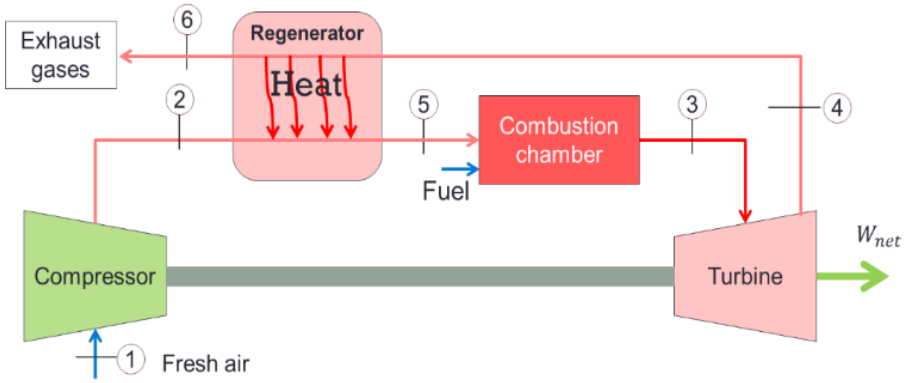


Figure 3. Schematic of regenerative gas turbine cycle

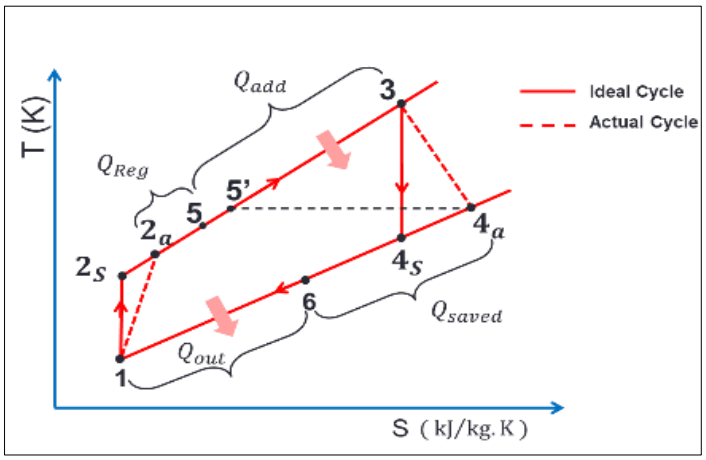


Figure 4. T-S diagram of the regenerative Brayton cycle showing ideal and actual processes

The regenerator effectiveness (ε) is defined using a temperature-based formulation:

$$\varepsilon = \frac{T_5 - T_2}{T_4 - T_2} \Longrightarrow T_5 = T_2 + \varepsilon(T_4 - T_2) \qquad (16)$$

Pressure losses within the regenerator are modeled independently for the cold and hot streams using a fixed pressure-drop ratio of 2% ($P_{d,reg} = 0.02$) on each side (Figure 5.)

$$P_5 = P_2\left(1 - P_{d,reg}\right), \qquad P_6 = P_4(1 - P_{d,reg}) \qquad (17)$$

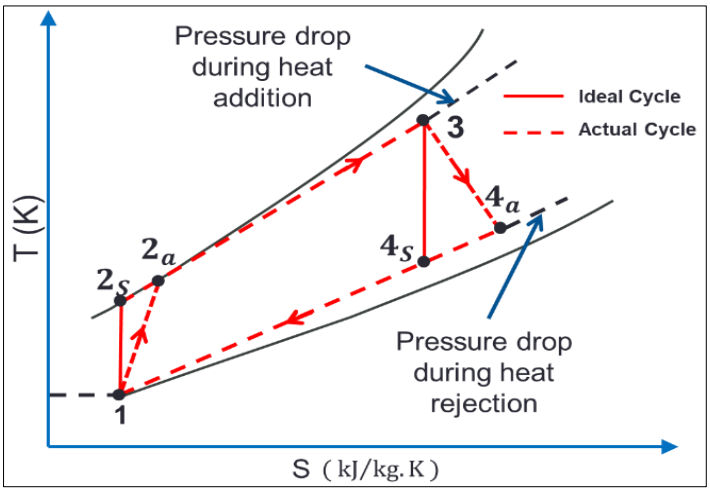


Figure 5. Actual Brayton cycle with irreversibilities

With the regenerator integrated, the compressed air is preheated to state 5, reducing the external thermal energy required in the combustion chamber. The updated fuel mass flow rate $\dot{m}_{f,reg}$ is calculated via a steady-flow energy balance across the combustor, substituting the compressor discharge enthalpy h_2 with the regenerator outlet enthalpy h_5.

$$\dot{m}_{f,reg} = \frac{\dot{m}_a(h_3 - h_5)}{\eta_{comb} \times LHV_{CH_4} - \left(h_3 - h_f\right)} \qquad (18)$$

The total combustion gas mass flow rate $\dot{m}_{g,reg}$ is then updated to reflect this new fuel-to-air mixture.

$$\dot{m}_{g,reg} = \dot{m}_a + \dot{m}_{f,reg} \qquad (19)$$

An energy balance across the counterflow regenerator determines the final enthalpy h_6 and temperature T_6 of the exhaust gases exiting to the atmosphere.

$$h_6 = h_4 - \frac{\dot{m}_a(h_5 - h_2)}{\dot{m}_{g,reg}} \qquad (20)$$

The recovered thermal energy Q_{saved} quantifies the exhaust heat successfully recycled back into the cycle.

$$Q_{saved} = \dot{m}_a(h_5 - h_2) \qquad (21)$$

The model subsequently calculates the regenerative turbine work, net cycle power output, and total heat input using these updated flow and enthalpy values.

$$\dot{W}_{turb,reg} = \dot{m}_{g,reg}(h_3 - h_4) \qquad (22)$$

$$\dot{W}_{net,reg} = \dot{W}_{turb,reg} - \dot{W}_{comp} \qquad (23)$$

$$Q_{in,reg} = \dot{m}_{f,reg} \times LHV_{HC_4} \times \eta_{comb} \qquad (24)$$

$$\eta_{th,reg} = \frac{\dot{W}_{net,reg}}{\dot{Q}_{in,reg}}, \qquad SFC = \frac{3600 \times \dot{m}_{f,reg}}{\dot{W}_{net,reg}} \qquad (25)$$

2.3. Plant Specifications and Model Validation

The thermodynamic models were applied to the GT13DM gas-turbine unit operated by the General Electricity Company of Libya at the Southern Tripoli Power Plant. Representative operating specifications and design parameters (Table 1) were implemented directly into the EES model.

Table 1. Operating parameters used in the thermodynamic simulations of the GT13DM gas-turbine unit

Parameters	Values	Units
Pressure ratio (r_p)	**11.5**	**–**
Turbine inlet temperature (TIT or T_3)	**990**	**°C**
Compressor inlet volumetric flow rate ($\dot{V}$)	**337.6**	**m³/s**
Compressor isentropic efficiency (η_c)	**0.84**	**–**
Turbine isentropic efficiency (η_t)	**0.89**	**–**
Lower heating value (LHV_{HC_4})	**50,023**	**kJ/kg**
Combustion efficiency (η_{comb})	**0.99**	**–**
Regenerator effectiveness§ (ε)	**0.80**	**–**

§*The nominal design-point assumption for the recuperator model, rather than as a value independently established through experimental validation of the recuperator.*

Table 2a. Technical specifications of the Southern Tripoli GT13DM gas-turbine unit

Power station	Unit	Year in service	Unit type	Nameplate rating	Available power	Model
Tripoli South	**GT-13DM**	**1994**	**Gas turbine**	**100 MW**	**85 MW**	**GT13DM**

To ensure the reliability of the thermodynamic framework, the baseline SGT model was validated against the nominal specifications of the GT13DM unit. Under winter reference conditions (16.21°C), the model predicts a net power output of 96.58 MW. This aligns closely with the plant's nameplate available power rating of 85–100 MW (Table 2a, b), confirming that the chosen isentropic efficiencies, pressure drops, and variable specific heat assumptions accurately reflect the real-world aerothermal behavior of the asset.

In general, the selected assumptions regarding isentropic efficiencies, pressure drops, and variable specific heat accurately reflect the actual thermodynamic (aerothermal) behavior of the equipment. Furthermore, across the range of ambient conditions studied, the model predicts an average power degradation rate of approximately 0.77 $MW/℃$ $(or \approx 0.80\ \%/℃$ relative to the base power). This result aligns closely with the typical degradation rate of $0.70\% - 0.85\%/℃$ as cited in manufacturer specifications and industry references for heavy-duty gas turbines [13, 18].

Table 2b. Validation of the GT13DM thermodynamic model against reference performance data at discrete ambient temperatures.

Condition / Ambient Temp (Ta)	Metric	Reference / OEM Data	EES Model (This Work)	Relative Error (%)
Winter Reference 16.21℃	Net Power (W_{net})	96.50MW	96.58MW	%0.08+
	Thermal Efficiency (η_{th})	%29.00	%28.86	%0.48-
ISO / Intermediate 26.15 ℃	Net Power (W_{net})	89.20MW	88.90MW	%0.33-
	Thermal Efficiency (η_{th})	%28.30	%28.25	%0.18-
Summer Peak 39.40 ℃	Net Power (W_{net})	79.50MW	78.67MW	%1.04-
	Thermal Efficiency (η_{th})	%27.50	%27.37	%0.47-

2.4. Emission Assessment

Combustion-related emissions were evaluated using a comparative thermodynamic-indicator approach. Fuel-based CO_2 emissions were estimated directly from the methane fuel-consumption rate using a standard mass-conservation approach:

$$\dot{m}_{CO_2} = \dot{m}_f \times EF_{CO_2} \qquad (26)$$

where the emission factor is:

$EF_{CO_2} = 2.74\ \text{kg CO}_2/\text{kg CH}_4 4$

The influence of regeneration on nitrogen oxides (NOx) and carbon monoxide (CO) formation was interpreted qualitatively using variations in the air–fuel ratio (AFR) and equivalence ratio (ϕ):

$$AFR = \frac{\dot{m}_a}{\dot{m}_f} \quad , \qquad \phi = \frac{AFR_{stoich}}{AFR} \qquad (27)$$

Because the present framework relies on bulk fluid thermodynamic states and does not resolve local adiabatic flame temperatures or detailed chemical kinetics, these parameters serve strictly as qualitative comparative indicators of emission propensity.

2.5. Ambient Temperature Distribution and Annual Weighting Procedure

Ambient air temperature (T_a) serves as the primary environmental variable governing cycle aerodynamics. High-resolution hourly ambient temperature records for the Tripoli South site (Latitude: 32.83° N, Longitude: 13.18° E) were obtained from the NASA Prediction of Worldwide Energy Resources (POWER) database, covering a representative full-year baseline period from January 2025 to December 2025 (totaling 8,736 operational hours). The recorded temperature domain was subsequently discretized into N = 8 discrete temperature bins using a standard bin-counting methodology (Table 3).

Table 3. Ambient Temperature Distribution, Occurrence Frequencies, Annual Operating Hours, and Weighting Factors

Bin (i)	Local Ambient Temperature T_a(°C)‡	Climatological Frequency (days)	Annual Operational Duration (h)	Normalized Weight Factor
1	12.9–16.21	37	888	0.1016
2	19.53	55	1,320	0.1511
3	22.84	38	912	0.1044
4	26.15	48	1,152	0.1319
5	29.46	69	1,656	0.1896
6	32.78	73	1,752	0.2005
7	36.09	30	720	0.0824
8	39.40	14	336	0.0385
Total		364	8,736	1.0000

‡*Source: https://power.larc.nasa.gov/data-access-viewer*

Each temperature bin was assigned an occurrence frequency ($Freq_i$), which was converted into annual operating hours ($Hours_i = Freq_i \times 24$) and normalized weighting factors ($Weight_i$). For each discrete ambient-temperature condition, the complete Brayton-cycle model was solved independently. To preserve dimensional and thermodynamic consistency, integrated performance quantities were evaluated using cumulative energy- and mass-weighted formulations. Total annual fuel

consumption ($fuel_{annual,kg}$) and cumulative net work output ($W_{net,annual}$) were calculated as:

$$fuel_{annual,kg} = \sum_{i=1}^{N} \left(\dot{m}_{f,i} \times 3600 \times Hours_i \right) \quad (28)$$

$$W_{net,annual} = \sum_{i=1}^{N} \left(\dot{W}_{net,i} \times Hours_i \right) \quad (29)$$

Accordingly, the annual thermal efficiency ($\eta_{thermal,annual}$) was evaluated from cumulative energy quantities:

$$\eta_{thermal,annual} = \frac{\sum_{i=1}^{N} (\dot{W}_{net,i} \times Hours_i)}{\sum_{i=1}^{N} (\dot{Q}_{in,i} \times Hours_i)} \quad (30)$$

This methodology captures the influence of ambient climatic variability on cycle behavior without introducing transient operation or part-load control dynamics.

3. Results

3.1. Ambient-Temperature-Driven Aerothermal Derating

The operational baseline of the GT13DM gas turbine is fundamentally constrained by seasonal atmospheric variations at the compressor intake. Because the compressor operates at a fixed volumetric capacity ($\dot{V} = 337.6\ m^3/s$), the mass flow rate is strictly a function of ambient air density.

Table 4 quantifies the thermodynamic consequences of seasonal ambient-temperature variation on the GT13DM gas turbine. Increasing ambient temperature reduces inlet air density and compressor mass flow rate, resulting in lower turbine work output and significant net power derating. The data also show a deterioration in thermal efficiency and an increase in specific fuel consumption under summer conditions. These results directly address the influence of climate on gas-turbine performance and establish the baseline for evaluating regeneration.

Figure 6 illustrates the direct dependence of compressor inlet-air density and mass flow rate on ambient temperature. As temperature increases, reduced air density lowers the quantity of working fluid entering the compressor at a fixed volumetric flow rate. This density-driven reduction in throughput represents the primary mechanism responsible for subsequent performance degradation. The figure therefore provides the fundamental aerodynamic explanation for ambient temperature sensitivity in the gas turbine.

Figure 6 quantifies this aerodynamic limitation. As ambient temperature (T_a) increases from the winter reference (16.21°C) to the summer extreme (39.40°C), the inlet air density drops from 1.220 kg/m ^{3} to 1.129 kg/m ^{3}. This 7.46% reduction in density directly translates to a proportional 7.53% decline in the absolute air mass

flow rate ($\dot{m}_a$), restricting the working fluid available for expansion.

This mass flow restriction induces a severe divergence between compression requirements and expansion output, as evidenced in Figure 7. While the gross turbine work ($\dot{W}_{turb}$) decreases by 7.53% due to the diminished mass flow, the absolute compressor work ($\dot{W}_{comp}$) decreases marginally by 0.12%. This occurs because the specific compression work required to overcome the temperature-dependent enthalpy barrier scales with T_1, overpowering the mass flow reduction. Consequently, the net power output ($\dot{W}_{net}$) suffers a compounded derating of 18.54% (from 96.58 MW to 78.67 MW). For the Libyan grid, this data highlights a critical vulnerability: the asset loses over one-fifth of its generating capacity precisely during peak summer cooling demand.

3.2. Influence of Ambient Temperature on Thermodynamic Performance

The aerothermal derating directly degrades the cycle's energy conversion effectiveness. Figure 10 demonstrates that the compressor discharge temperature (T_2) rises linearly with ambient temperature, reaching 404.2 °C at peak summer conditions. While this elevated T_2 slightly reduces the sensible heat addition required in the combustor, reflected by the marginal decline in fuel mass flow ($\dot{m}_f$) in Figure 9, this fuel saving is vastly disproportionate to the 18.54% loss in power output.

As a result, Figure 8 shows a distinct deterioration in overall performance: thermal efficiency (η_{th}) decreases from 28.86% to 27.37%, while SFC increases from 0.2519 to 0.2656 kg/kWh. These graphical trends confirm that lower absolute fuel consumption during summer operations is merely an artifact of reduced cycle capacity, not an indicator of improved efficiency.

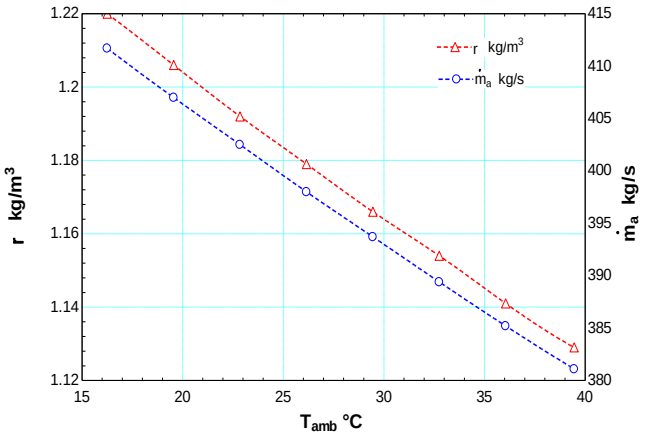


Figure 6 Variation of inlet-air density and compressor air mass flow rate versus ambient temperature

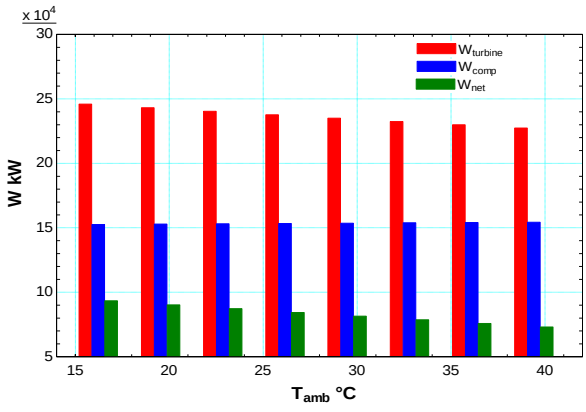


Figure 7 Variation of compressor work, turbine work, and net power output versus ambient temperature for the simple cycle

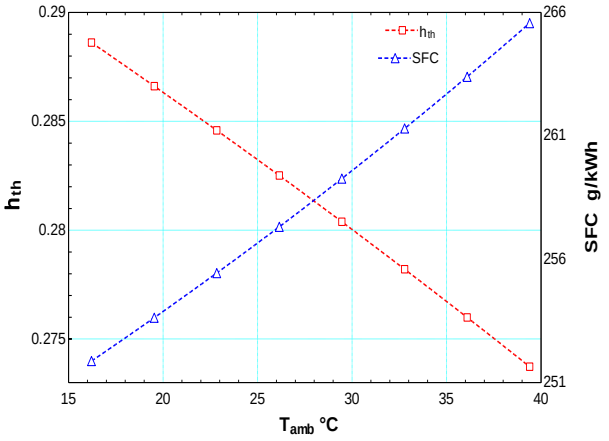


Figure 8: Thermal efficiency and specific fuel consumption versus ambient temperature

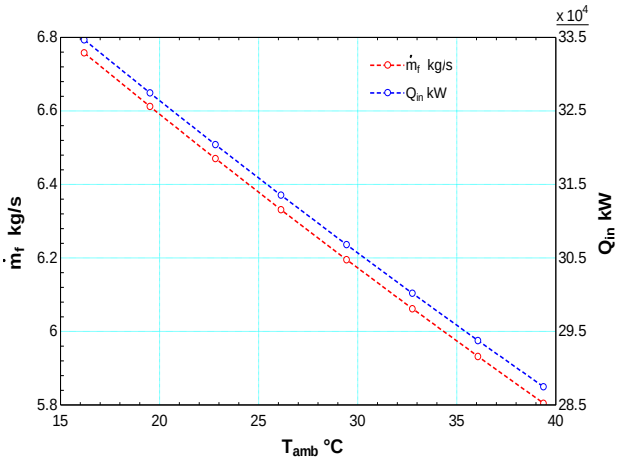


Figure 9: Fuel mass flow rate and total heat input versus ambient temperature

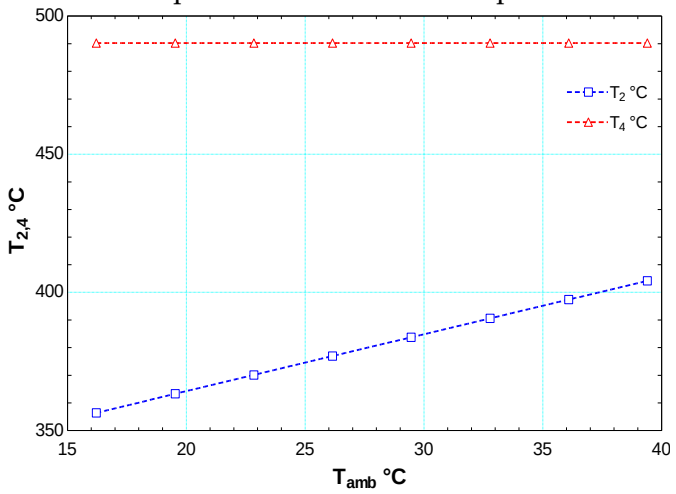


Figure 10 Variation of compressor discharge temperature (T_2) and turbine exhaust temperature (T_4) versus ambient temperature

Table 4. Summary of principal thermodynamic state points and performance indicators at representative winter and summer operating conditions

Parameter	Symbol	Unit	Winter Condition $T_a = 16.21$℃	Summer Condition $T_a = 39.40$℃	Change (%)
Compressor inlet air density	ρ_1	kg/m^3	1.22	1.129	-7.46%
Compressor air mass flow rate	$\dot{m}_a$	Kg/s	411.7	386.9	-7.53%
Compressor work	$\dot{W}_{comp}$	kW	143,564	143,393	-0.12%
Turbine work	$\dot{W}_{turb}$	kW	240,144	222,067	-7.53%
Net cycle power output	$\dot{W}_{net}$	kW	96,580	78,674	-18.54%
Compressor outlet temperature	T_2	$°C$	356.4	404.2	13.41%
Turbine exhaust temperature	T_4	$°C$	490.2	490.2	0.00%
Fuel mass flow rate	$\dot{m}_f$	Kg/s	6.757	5.804	-14.10%
Thermal energy input	$\dot{Q}_{in}$	MW	335	287	-14.33%
Thermal efficiency	η_{th}	%	28.86	27.37	-5.16%
Specific fuel consumption	SFC	g/kWh	251.9	265.6	5.44%

3.3. Performance Comparison of Simple and Regenerative Cycles

Integrating a regenerator fundamentally shifts the cycle's heat addition boundary conditions. Figures 11 and 12 demonstrate that the RGT configuration consistently outperforms the SGT, maintaining higher thermal efficiency and lower SFC across the entire ambient spectrum. By recycling high-grade exhaust enthalpy to preheat the compressor discharge air, the RGT requires significantly less chemical energy to achieve the 990°C TIT.

Table 5. Percentage improvements achieved through regeneration at selected ambient temperatures at Regenerator Effectiveness, $\varepsilon = 80\ \%$

Ambient Temperature, T_a °C	Thermal Efficiency Improvement (%)	Reduction in Specific Fuel Consumption (%)	Relative Change in Net Power Output (%)
16.21	16.49%	14.172%	-2.197%
19.53	15.60%	13.486%	-2.203%
22.84	14.69%	12.803%	-2.208%
26.15	13.77%	12.087%	-2.213%
29.46	12.84%	11.415%	-2.218%
32.78	11.93%	10.677%	-2.225%
36.09	11.01%	9.909%	-2.230%
39.40	10.08%	9.149%	-2.237%

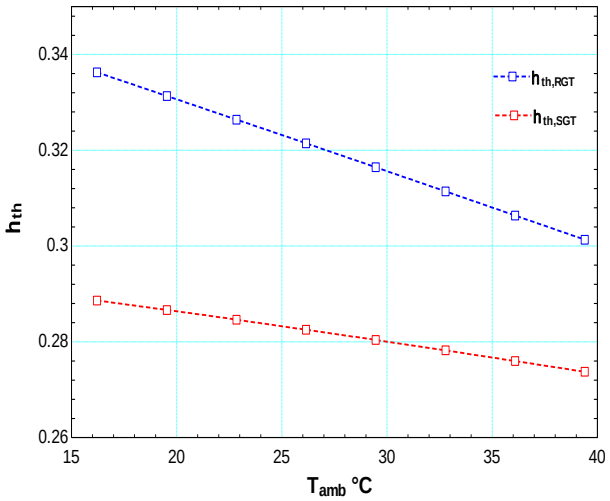


Figure 11 Comparison of SGT and RGT thermal efficiency versus ambient temperature

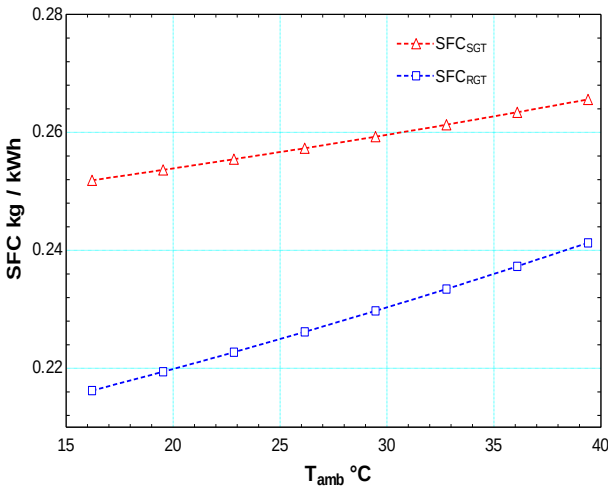


Figure 12 Comparison of SGT and RGT specific fuel consumption versus ambient temperature

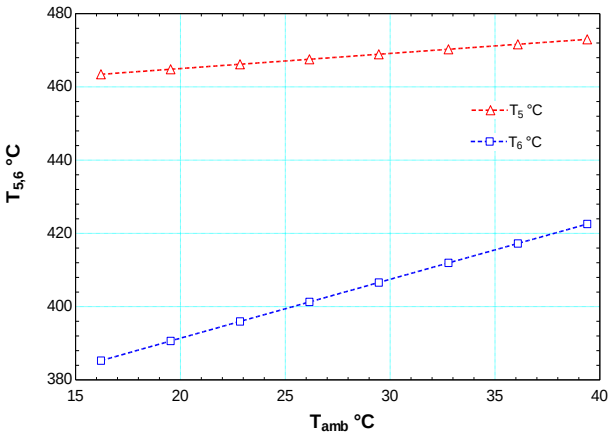


Figure 13 Variation of regenerator outlet temperature (T_5) and exhaust exit temperature (T_6) versus ambient temperature

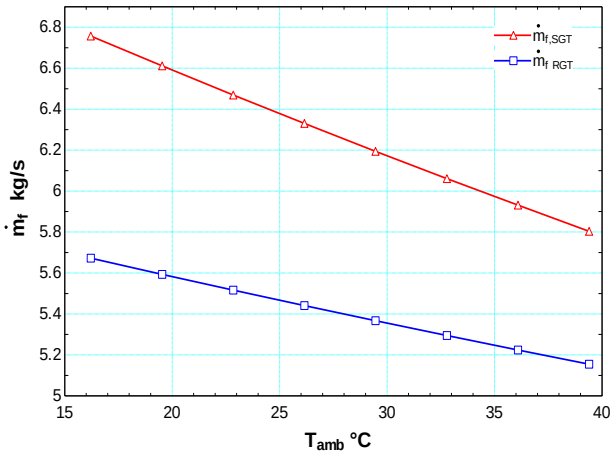


Figure 14 Comparison of SGT and RGT fuel mass flow rates versus ambient temperature

However, Figure 11 reveals a critical thermodynamic limitation: the performance gap between the RGT and SGT narrows as ambient temperature rises. Table 5 quantifies this convergence, showing the relative efficiency improvement degrading from 16.49% at 16.21°C to 10.08% at 39.40°C. This behavior is explained by the temperature profiles in Figure 13. As T_a rises, T_2 also rises, which narrows the available thermal gradient ($T_4 - T_2$) across the regenerator. This thermodynamic pinch restricts the heat recovery potential during peak summer conditions, indicating that regeneration is most effective during cooler operational periods.

3.4. Sensitivity and Uncertainty of Cycle Parameters

Tables 6.1–6.5 evaluate the sensitivity of cycle performance to increasing regenerator effectiveness. Higher effectiveness values increase compressed-air preheating, resulting in improved thermal efficiency and lower fuel consumption. The results also reveal diminishing incremental benefits as effectiveness approaches practical upper limits.

Table 6.1 Sensitivity metrics showing incremental performance improvements for different values of regenerator effectiveness. Regenerator Effectiveness, $\varepsilon = 0.00$

T_{amb} °C	T_5 °C	T_6 °C	η_{th} %	%Δ η_{th}	SFC kg/kWh	%Δ SFC	$\dot{m}_f$ kg/s	%Δ $\dot{m}_f$
16.21	–	–	0.2886	–	0.2519	–	6.757	–
19.53	–	–	0.2866	–	0.2536	–	6.611	–
22.84	–	–	0.2846	–	0.2554	–	6.469	–
26.15	–	–	0.2825	–	0.2573	–	6.33	–
29.46	–	–	0.2804	–	0.2593	–	6.194	–
32.78	–	–	0.2782	–	0.2613	–	6.061	–
36.09	–	–	0.276	–	0.2634	–	5.931	–
39.40	–	–	0.2737	–	0.2656	–	5.804	–

($T5$): Regenerator Outlet Temperature

($T6$): Exhaust Exit Temperature

(η_{th}): Thermal Efficiency, ($\%\Delta\,\eta_{th}$): Percentage improvement in thermal efficiency

(SFC): Specific Fuel Consumption, ($\%\Delta\,SFC$): Reduction in specific fuel consumption.

($\dot{m}_f$): Fuel Mass Flow Rate, ($\%\Delta\,\dot{m}_f$): Percentage fuel saving.

Table 6.2 Sensitivity metrics showing incremental performance improvements for different values of regenerator effectiveness. Regenerator Effectiveness, $\varepsilon = 70$ %

T_{amb} ℃	T_5 °C	T_6 °C	η_{th} %	$\%\Delta\,\eta_{th}$	$SFC\ kg/kWh$	$\%\Delta\,SFC$	$\dot{m}_f\ kg/s$	$\%\Delta\,\dot{m}_f$
16.21	421.2	383.3	0.3286	13.86%	0.2212	12.19%	5.810	14.02%
19.53	423.3	388.0	0.3241	13.08%	0.2243	11.55%	5.722	13.45%
22.84	425.3	392.6	0.3197	12.33%	0.2274	10.96%	5.636	12.88%
26.15	427.4	397.3	0.3152	11.58%	0.2306	10.38%	5.553	12.27%
29.46	429.4	401.9	0.3106	10.77%	0.234	9.76%	5.471	11.67%
32.78	431.4	406.5	0.306	9.99%	0.2375	9.11%	5.391	11.05%
36.09	433.5	411.2	0.3014	9.20%	0.2412	8.43%	5.313	10.42%
39.40	435.5	415.8	0.2968	8.44%	0.2449	7.79%	5.236	9.79%

Table 6.3 Sensitivity metrics showing incremental performance improvements for different values of regenerator effectiveness. Regenerator Effectiveness, $\varepsilon = 75$ %

T_{amb} ℃	T_5 °C	T_6 °C	η_{th} %	$\%\Delta\,\eta_{th}$	$SFC\ kg/kWh$	$\%\Delta\,SFC$	$\dot{m}_f kg/s$	$\%\Delta\,\dot{m}_f$
16.21	456.7	392.0	0.3324	15.18%	0.2187	13.18%	5.741	15.04%
19.53	458.5	397.0	0.3277	14.34%	0.2218	12.54%	5.658	14.42%
22.84	460.2	402.0	0.323	13.49%	0.2251	11.86%	5.576	13.80%
26.15	461.9	406.9	0.3183	12.67%	0.2284	11.23%	5.497	13.16%
29.46	463.6	411.9	0.3135	11.80%	0.2319	10.57%	5.419	12.51%
32.78	465.3	416.9	0.3087	10.96%	0.2355	9.87%	5.343	11.85%
36.09	467.0	421.9	0.3039	10.11%	0.2392	9.19%	5.268	11.18%
39.40	468.7	426.8	0.299	9.24%	0.2431	8.47%	5.196	10.48%

Table 6.4 Sensitivity metrics showing incremental performance improvements for different values of regenerator effectiveness. Regenerator Effectiveness, $\varepsilon = 80\%$

T_{amb} ℃	T_5 °C	T_6 °C	η_{th} %	%Δ η_{th}	$SFC\ kg/kWh$	%Δ SFC	$\dot{m}_f\ kg/s$	%Δ $\dot{m}_f$
16.21	463.40	385.30	0.3362	16.49%	0.2162	14.17%	5.673	16.04%
19.53	464.80	390.60	0.3313	15.60%	0.2194	13.49%	5.593	15.40%
22.84	466.20	395.90	0.3264	14.69%	0.2227	12.80%	5.516	14.73%
26.15	467.50	401.30	0.3214	13.77%	0.2262	12.09%	5.441	14.04%
29.46	468.90	406.60	0.3164	12.84%	0.2297	11.42%	5.367	13.35%
32.78	470.30	411.90	0.3114	11.93%	0.2334	10.68%	5.294	12.65%
36.09	471.60	417.20	0.3064	11.01%	0.2373	9.91%	5.224	11.92%
39.40	473.00	422.50	0.3013	10.08%	0.2413	9.15%	5.155	11.18%

Table 6.5 Sensitivity metrics showing incremental performance improvements for different values of regenerator effectiveness. Regenerator Effectiveness, $\varepsilon = 85\ \%$

T_{amb} ℃	T_5 °C	T_6 °C	η_{th} %	%Δ η_{th}	$SFC\ kg/kWh$	%Δ SFC	$\dot{m}_f\ kg/s$	%Δ $\dot{m}_f$
16.21	470.10	378.50	0.3402	17.88%	0.2137	15.16%	5.604	17.06%
19.53	471.20	384.20	0.335	16.89%	0.217	14.43%	5.529	16.37%
22.84	472.20	389.90	0.3299	15.92%	0.2204	13.70%	5.456	15.66%
26.15	473.20	395.60	0.3247	14.94%	0.2239	12.98%	5.384	14.94%
29.46	474.20	401.20	0.3194	13.91%	0.2276	12.23%	5.315	14.19%
32.78	475.30	406.90	0.3142	12.94%	0.2314	11.44%	5.246	13.45%
36.09	476.30	412.60	0.3089	11.92%	0.2353	10.67%	5.179	12.68%
39.40	477.30	418.20	0.3036	10.92%	0.2394	9.86%	5.114	11.89%

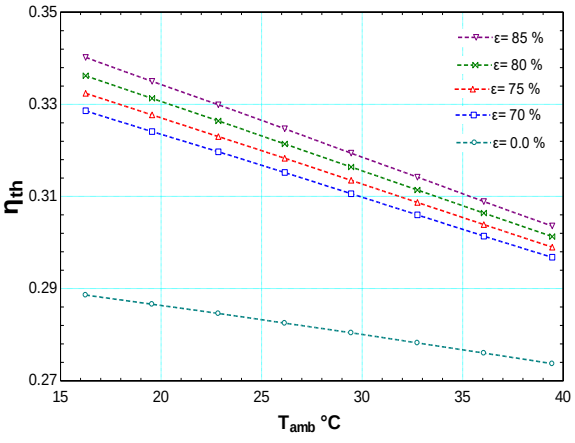


Figure 15 Thermal efficiency versus regenerator effectiveness (ε)

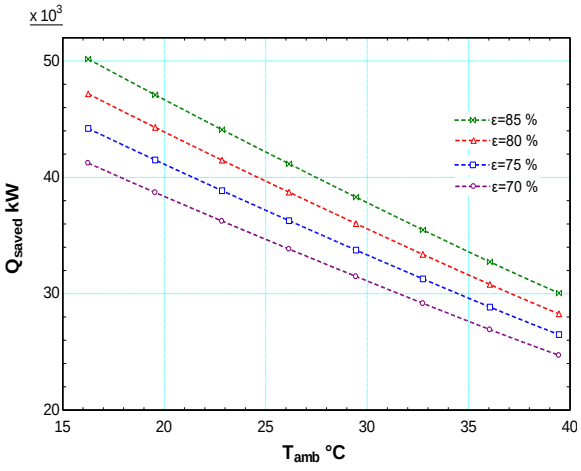


Figure 17 Recovered heat-transfer rate and fuel-saving percentage versus regenerator effectiveness

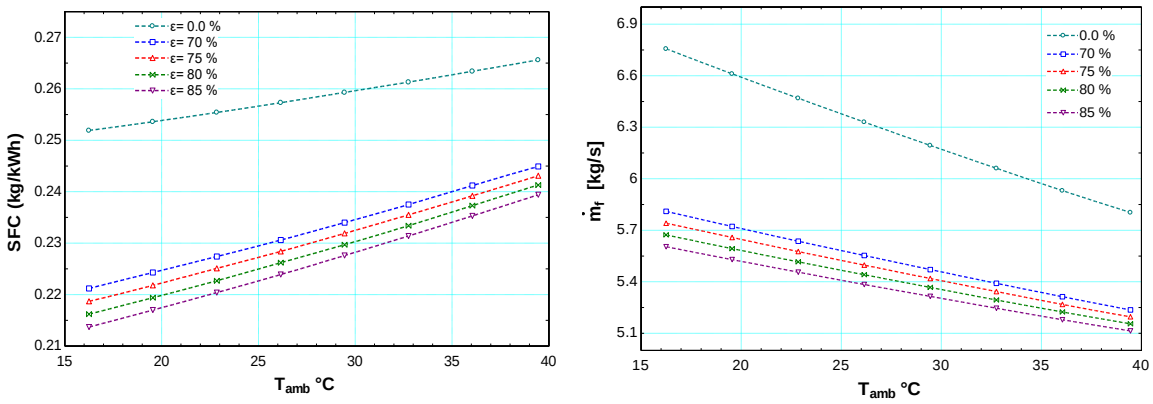


Figure 16 Specific fuel consumption versus regenerator effectiveness (ε)

To avoid overly deterministic claims based on fixed assumptions, it is necessary to address the sensitivity of the model. The baseline framework assumes fixed isentropic efficiencies ($\eta_c = 0.84, \eta_t = 0.89$) and constant fractional pressure drops. In reality, component degradation (e.g., compressor fouling, turbine blade erosion) will alter these parameters over the asset's lifecycle, introducing uncertainty into the absolute power and efficiency predictions. However, because the primary mechanism of the RGT, exhaust heat recovery, operates independently of turbomachinery isentropic efficiency, the relative performance improvements reported in this study remain robust regardless of baseline degradation.

Figures 15 through 17 evaluate the sensitivity of the cycle to regenerator effectiveness (ε). While thermal efficiency increases monotonically with higher effectiveness, the asymptotic flattening of the curves in Figures 15 and 16 indicates diminishing thermodynamic returns. As ε approaches 0.85, the preheated air temperature (T_5) approaches the turbine exhaust temperature (T_4). Pushing effectiveness beyond 0.80 requires exponentially larger heat exchanger surface areas to overcome the narrowing thermal pinch point, which increases pressure drops and capital costs. Therefore, the selected $\varepsilon = 0.80$ represents a pragmatic techno-economic boundary for retrofitting.

Figures 15 through 17 evaluate the sensitivity of the cycle to regenerator effectiveness (ε). While thermal efficiency increases monotonically with higher effectiveness, the asymptotic flattening of the curves in Figures 15 and 16 indicates diminishing thermodynamic returns. As ε approaches 0.85, the preheated air temperature (T_5) approaches the turbine exhaust temperature (T_4). Pushing effectiveness beyond 0.80 requires exponentially larger heat exchanger surface areas to overcome the narrowing thermal pinch point, which increases parasitic pressure drops and capital expenditures.

In industrial practice and heavy-duty gas turbine applications, regenerator effectiveness values between 0.75 and 0.85 are widely recognized as the optimal techno-economic compromise between exergy recovery and equipment footprint

[15, 17, 20, 33]. Therefore, the selected ε = 0.80 represents a pragmatic, industry-standard techno-economic boundary for retrofitting existing installations.

3.5. Annualized Performance Assessment under Southern Tripoli Climatic Conditions

Table 7 presents annualized performance indicators obtained using the Southern Tripoli temperature frequency distribution. The results show that regeneration significantly improves annual thermal efficiency while reducing fuel consumption and carbon emissions. Net electrical energy production remains nearly unchanged, indicating that the primary benefit of regeneration is improved fuel utilization rather than increased power generation. The table therefore quantifies the long-term operational advantages of regenerative integration.

Table 7. Annual weighted performance metrics for SGT and RGT configurations.

Performance Metric	Simple Cycle	Regenerative Cycle	Absolute Change	Relative Change (%)
Net Electrical Generation (MWh)	768,300	751,300	−17,000	−2.21%
Annual Heat Input (MWh)	2,725,000	2,346,000	−379,000	−13.91%
Annual Thermal Efficiency (%)	28.20%	32.02%	+3.82 percentage points	+13.55%
Annual Fuel Consumption (ton/year)	198,061	170,550	−27,511	−13.89%
Specific Fuel Consumption (g/kWh)	257.8	227.0	−30.8	−11.95%
Annual Fuel Expenditure (USD)	13,270,087	11,426,850	−1,843,237	−13.89%
CO_2 Emissions (ton)	542,687	467,306	−75,381	−13.89%
CO_2 Emission Intensity (g/kWh)	706.3	622.0	−84.3	−11.93%

Table 8 summarizes the cumulative annual benefits associated with regeneration. The results indicate substantial reductions in fuel consumption and corresponding decreases in carbon dioxide emissions. These savings demonstrate the practical economic and environmental value of exhaust-heat recovery under representative Libyan climatic conditions. The table translates thermodynamic improvements into annual operational outcomes.

Table 8. Annual fuel savings and percentage reductions achieved through regeneration.

Indicator	Symbol	Unit	Value
Annual fuel consumption (SGT)	$Fuel_{annual,SGT}$	ton/year	198,061
Annual fuel consumption (RGT)	$Fuel_{annual,RGT}$	ton/year	170,550
Annual fuel savings	$\Delta\, Fuel_{annual}$	ton/year	27,511
Fuel saving percentage	$Fuel_{saving}$	%	13.89%
Annual CO_2 emissions (SGT)	$CO_{2,annual,SGT}$	ton/year	542,687
Annual CO_2 emissions (RGT)	$CO_{2,annual,RGT}$	ton/year	467,306
Annual CO_2 reduction	$\Delta\, CO_{2,annual}$	ton/year	75,381
CO_2 reduction percentage	$CO_{2,reduction}$	%	13.89%

 https://doi.org/10.37375/ijer.v5i1 *Vol. 5(1), October 2026*

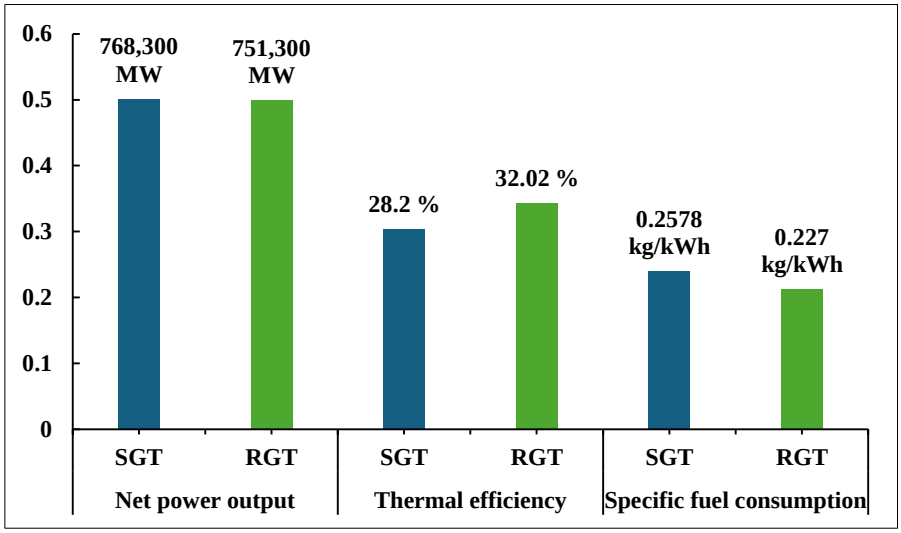


Figure 18: Annual weighted comparison of SGT and RGT net power output, thermal efficiency, and specific fuel consumption

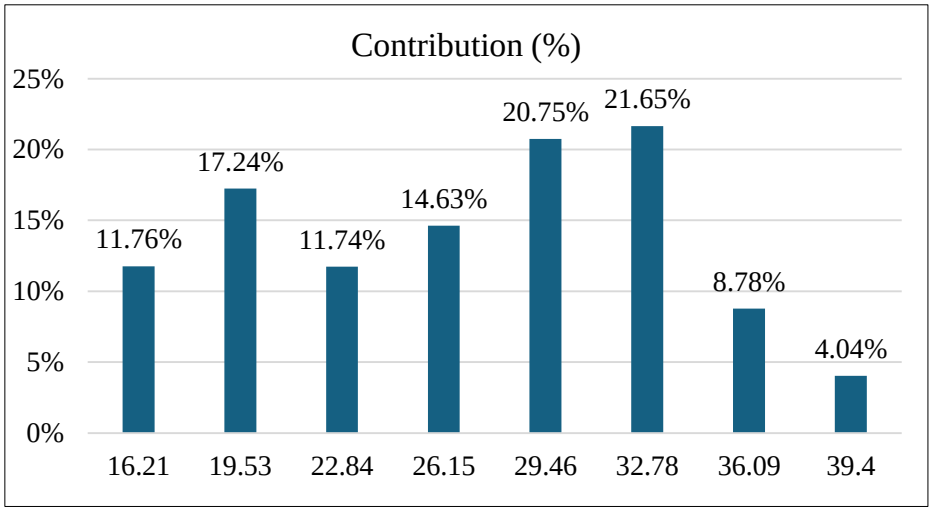


Figure 19 Contribution of each temperature bin to annual fuel consumption

The primary methodological novelty of this study lies in transitioning from discrete design-point analyses to an annualized, meteorologically weighted performance assessment. By integrating the steady-state results across the 8,736-hour climatic profile of Southern Tripoli (Table 3), the true operational value of the RGT retrofit is quantified.

Figure 18 demonstrates that while the annual net power output remains virtually identical between the two cycles (since regeneration does not alter the mass flow limitations), the annualized thermal efficiency increases substantially from 28.2% to 32.02%. Figure 19 illustrates that moderate-to-high ambient temperatures dominate the plant's annual fuel budget due to their high occurrence frequency. By implementing regeneration, the plant achieves a 13.89% reduction in annual fuel consumption, saving approximately 27.51 million kg of natural gas (Table 8). This confirms that the primary benefit of the RGT is a drastic improvement in energy conversion effectiveness, directly relieving fuel supply chain pressures.

3.6. Environmental Impact and Combustion Boundary Shifts

Table 9 evaluates the environmental implications of regenerative integration using annualized fuel consumption and combustion-related indicators. Regeneration lowers annual fuel use and carbon dioxide emissions while increasing the air-fuel ratio and reducing the equivalence ratio. These changes indicate leaner combustion conditions with reduced carbon-emission intensity. The table therefore links thermodynamic improvements to broader environmental performance objectives.

Table 9. Annual fuel consumption, CO_2 emissions, and relative emission tendency indicators for SGT and RGT systems.

Emission Indicator	Unit	SGT	RGT	Relative Change (%)
Annual fuel consumption	$kg/year$	198,061	170,550	-13.89%
Annual carbon dioxide emissions $CO_{2,annual}$	$ton/year$	542,687	467,306	-13.89%
Annual weighted air–fuel ratio, AFR_{annual}	$kg\ air\ /kg\ fuel$	63.0865	73.2095	16.05%
Annual weighted equivalence ratio ϕ_{annual}	–	0.2727	0.2349	-13.86%
Annual weighted combustor inlet temperature	$°C$	378.8205	467.9067	23.52%

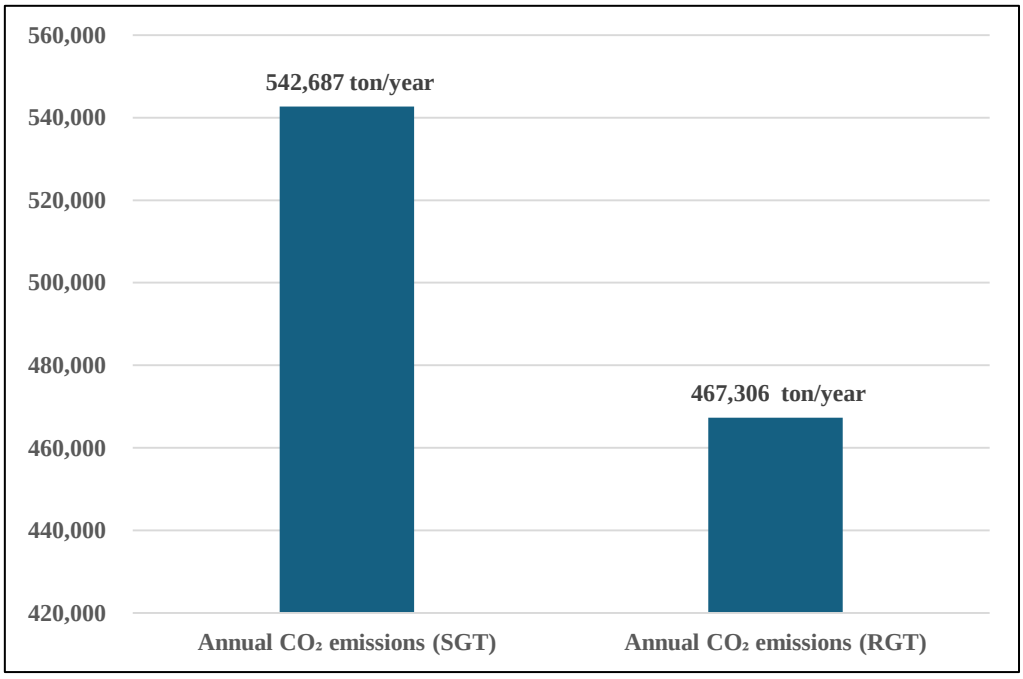


Figure 20: Annual CO_2 emissions of SGT and RGT configurations

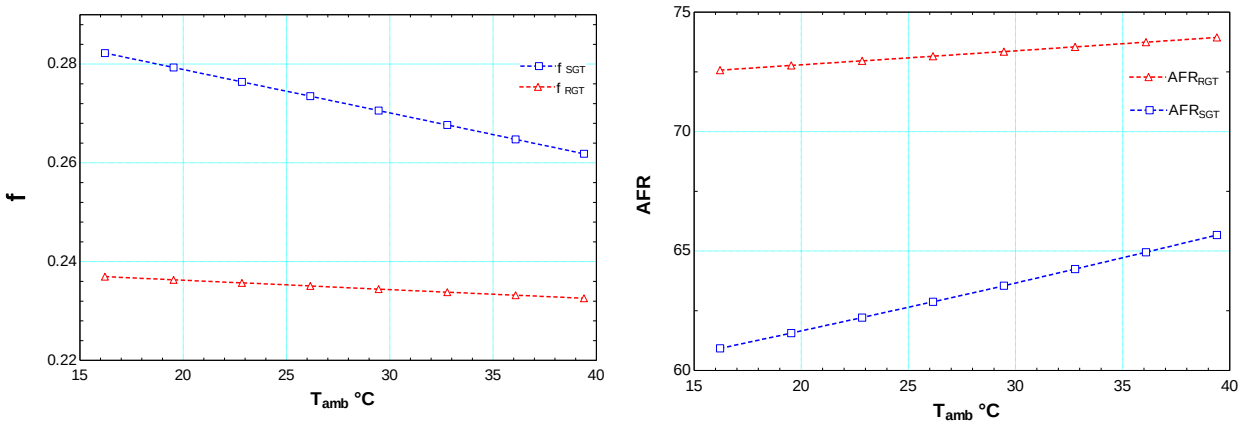


Figure 21: Variation of air-to-fuel ratio (AFR) and equivalence ratio (ϕ) with ambient temperature for SGT and RGT cycles

The thermodynamic improvements yield deterministic reductions in greenhouse gas emissions. Because CO_2 emissions are a stoichiometric consequence of fuel consumption, the RGT configuration prevents the release of 75,381 tons of CO_2 annually (Figure 20).

Regarding criteria pollutants (NOx and CO), absolute emission rates cannot be accurately predicted without detailed chemical kinetic modeling or computational fluid dynamics (CFD). However, Figure 21 provides critical insight into the shifts in combustion boundary conditions. Because the regenerator supplies preheated air, less fuel is injected into the same mass of air, driving the Air-to-fuel ratio (AFR) up and the equivalence ratio (ϕ) down (from an annual average of 0.2727 to 0.2349). While this leaner mixture typically reduces the propensity for incomplete oxidation (lowering CO formation), the elevated combustor inlet temperatures (T_5) associated with regeneration increase the risk of thermal NOx formation. Consequently, while the carbon footprint is definitively reduced, implementing an RGT retrofit would necessitate concurrent tuning of the plant's dry low-NOx (DLN) combustion systems to ensure regulatory compliance.

4. Discussion

4.1. Ambient Temperature as the Primary Driver of Gas Turbine Performance

Ambient temperature is the primary environmental parameter governing gas turbine performance because it directly determines compressor inlet-air density. As ambient temperature increases, the lower air density reduces the compressor air mass flow rate at a fixed volumetric intake, thereby limiting the working fluid available for expansion in the Brayton cycle. This reduction causes turbine work to decrease, while compressor work increases slightly because higher inlet temperatures require greater specific compression work. Consequently, the decline in turbine output exceeds the reduction in compressor demand, resulting in a pronounced deterioration in net power output. Although fuel consumption also

decreases due to the lower air throughput, the reduction is insufficient to offset the larger loss in power generation, leading to lower thermal efficiency and higher specific fuel consumption. These findings are consistent with established Brayton-cycle theory and previous studies on heavy-duty gas turbines operating in hot climates. The effect is particularly significant in North Africa and the Middle East, where high ambient temperatures coincide with peak electricity demand. Since component efficiencies and pressure losses were held constant, the observed performance degradation is attributed primarily to climatic conditions rather than mechanical deterioration.

4.2. Thermodynamic Benefits and Limitations of Regeneration

The regenerative gas turbine (RGT) enhances Brayton-cycle performance by recovering high-grade thermal energy from the turbine exhaust to preheat the compressed air before combustion, thereby improving exergy utilization and reducing the external heat addition required to achieve the prescribed turbine inlet temperature. Consequently, thermal efficiency increases because a greater proportion of the supplied fuel energy is converted into useful work, while specific fuel consumption decreases as less fuel is required to produce nearly the same net power output. The negligible change in power output reflects the fact that regeneration modifies the heat addition process rather than the compressor air mass flow rate or turbine expansion process, which remain governed by the same operating conditions. Thus, regeneration does not eliminate the ambient-temperature-induced power derating; rather, it partially offsets its impact on net power output relative to the simple-cycle configuration. However, the relative performance benefits diminish with increasing ambient temperature because higher compressor discharge temperatures reduce the available temperature difference between the turbine exhaust and compressed air, limiting heat recovery through the regenerator. This behavior is consistent with published studies on regenerative Brayton cycles, which report diminishing gains under hot-climate operation due to finite temperature differences and thermodynamic pinch-point constraints that inherently restrict maximum heat-transfer effectiveness.

4.3. Influence of Regenerator Effectiveness on Cycle Performance

Increasing regenerator effectiveness (ε) enhances thermal efficiency because a larger fraction of the turbine exhaust thermal energy is recovered to preheat the compressed air before combustion, thereby reducing the external fuel energy required to reach the prescribed turbine inlet temperature. Consequently, fuel consumption and specific fuel consumption decrease as a greater proportion of the available exhaust exergy is reutilized within the Brayton cycle. However, the incremental performance gains diminish at higher effectiveness values because the temperature difference between the exhaust gas and compressed air progressively decreases, reducing the driving force for heat transfer in accordance with second-law thermodynamics. Accordingly, $\varepsilon = 0.80$ is adopted as a representative high-

effectiveness value because it provides substantial heat recovery while avoiding the increasingly severe temperature-pinch, heat-transfer-area, pressure-loss, and cost penalties associated with effectiveness values approaching unity. This finite temperature difference imposes an inherent limit on heat recovery, making perfect regeneration unattainable due to unavoidable entropy generation and irreversible heat exchange. From an engineering perspective, increasing ε beyond approximately 0.80 requires disproportionately larger heat-transfer surfaces, resulting in higher capital cost, additional pressure losses, and increased system complexity. These trends are consistent with industrial regenerative gas turbine practice, where moderate effectiveness values are generally preferred to balance thermodynamic performance and economic feasibility, indicating that $\varepsilon \approx 0.80$ represents a practical target for retrofit applications in existing heavy-duty gas turbine installations.

4.4. Annual Performance Under Representative Libyan Climatic Conditions

Annual weighting is essential because gas turbines operate under continuously varying climatic conditions rather than at a single design-point temperature, making annual performance dependent on the frequency and duration of each ambient-temperature condition. The meteorologically weighted approach therefore provides a more realistic assessment of long-term operation by integrating performance over the complete annual temperature distribution. Intermediate temperature bins contribute most to annual performance because they occur for the greatest number of operating hours, whereas extreme winter and summer conditions, despite their influence on instantaneous performance, represent a smaller fraction of the annual operating period. Consequently, annual performance differs from design-point predictions, as cumulative energy production, fuel consumption, and thermal efficiency are governed by the statistical distribution of ambient conditions instead of isolated operating states. This methodology provides a more representative basis for evaluating long-term fuel utilization and operational efficiency, enabling utilities to quantify the practical benefits of regenerative retrofits under realistic climatic conditions. Such information supports maintenance scheduling, fuel procurement, and generation planning while improving the reliability of investment decisions. For electric utilities operating in hot-climate regions, annualized assessments provide a stronger foundation for optimizing plant performance, reducing operating costs, and enhancing long-term energy security.

4.5. Environmental Implications of Regeneration

The reduction in annual carbon dioxide emissions is a direct consequence of lower fuel consumption, since CO_2 formation from methane combustion is governed primarily by the carbon mass balance under complete-combustion conditions. By recovering turbine exhaust heat to preheat the compressed air, the regenerative cycle reduces the external heat input required to achieve the prescribed turbine inlet temperature and consequently lowers the required fuel flow. For the representative

climatic conditions considered in this study, the reduction in fuel consumption results in an annual CO_2 avoidance of approximately 75,381 tonnes relative to the simple-cycle configuration. Therefore, regeneration provides a direct pathway for reducing the carbon intensity of electricity generation without altering the fundamental operating principle of the gas turbine. These results demonstrate that regenerative retrofits can contribute to decarbonization by improving fuel utilization and reducing greenhouse-gas emissions from existing natural-gas-fired generation assets.

4.6. Engineering Significance, Practical Implications, and Future Research

This study contributes scientifically by providing a meteorologically weighted thermodynamic assessment of regenerative gas turbine performance under representative hot-climate operating conditions, extending conventional design-point analyses to annual operational evaluation. The results demonstrate that regeneration is an attractive retrofit option for existing GT13DM units because it significantly improves fuel utilization and thermal efficiency without requiring major modifications to the core turbomachinery. Such improvements can reduce operating costs, lower natural gas consumption, and decrease carbon emissions, thereby strengthening energy security in Libya by improving the efficiency of existing generating assets. The proposed methodology is also applicable to other heavy-duty gas turbines operating in hot-climate regions with similar environmental conditions. However, the present model is limited by its steady-state thermodynamic formulation and does not account for transient operation, component degradation, detailed combustion chemistry, or economic optimization, which should be addressed in future investigations.

5. Conclusion

This study evaluated the thermodynamic and environmental impacts of integrating a regenerator into the GT13DM gas turbine at the Southern Tripoli Power Plant. Moving beyond standard discrete-point Brayton cycle analyses, this research integrated steady-state thermodynamic modeling with high-resolution, site-specific meteorological weighting to provide a realistic assessment of retrofit feasibility in hot-climate regions. The principal findings are as follows:

Elevated ambient temperatures severely penalize the GT13DM. As temperatures rise from 16.21°C to 39.40°C, density-driven mass flow reductions cause an 18.54% derating in net power output, exacerbating grid vulnerabilities during peak summer demand.

The RGT configuration consistently outperforms the SGT by recycling exhaust heat. However, the relative efficiency advantage narrows from 16.49% in winter to 10.08% in summer due to a thermodynamic pinch effect at the regenerator, as elevated compressor discharge temperatures reduce the available heat recovery gradient.

When weighted against the specific climatic profile of Southern Tripoli, the RGT retrofit increases the annualized thermal efficiency from 28.20% to 32.02% and reduces specific fuel consumption by 11.95%. This translates to massive operational savings, conserving 27.51 million kg of natural gas annually.

The improved energy conversion effectiveness prevents the emission of over 75,381 tons of CO_2 per year. While leaner combustion conditions (ϕ_{annual} drops from 0.2727 to 0.2349) suggest favorable tendencies for CO reduction, the elevated combustor inlet temperatures highlight the necessity for careful NOx management during implementation.

Ultimately, these findings confirm that retrofitting existing gas turbine infrastructure with regenerators is a highly viable strategy. For the Libyan power sector, it offers a pragmatic, data-supported pathway to offset the adverse efficiency effects of hot climates, reduce fuel supply chain burdens, and advance grid sustainability without the prohibitive capital costs of combined-cycle infrastructure.

Nomenclature

Symbol	Definition	Unit
$\boldsymbol{AFR}$	Air-to-fuel ratio	kg air/kg fuel
$\boldsymbol{AFR_{annual}}$	Annual weighted air-to-fuel ratio	kg air/kg fuel
$\boldsymbol{AFR_{stoich}}$	Stoichiometric air-to-fuel ratio	kg air/kg fuel
$\boldsymbol{EF_{CO_2}}$	Carbon dioxide emission factor for methane combustion	kg CO_2/kg CH_4
$\boldsymbol{Freq_i}$	Occurrence frequency of ambient-temperature bin i	days
$\boldsymbol{Fuel_{annual,kg}}$	Annual fuel consumption	kg/year
$\boldsymbol{Fuel_{saving}}$	Annual fuel-saving percentage	%
$\boldsymbol{h}$	Specific enthalpy	kJ/kg
$\boldsymbol{h_f}$	Specific enthalpy of the fuel	kJ/kg
$\boldsymbol{Hours_i}$	Annual operating hours associated with temperature bin i	h
$\boldsymbol{i}$	Ambient-temperature-bin index	—
$\boldsymbol{LHV_{CH_4}}$	Lower heating value of methane fuel	kJ/kg
$\boldsymbol{\dot{m}_a}$	Compressor inlet air mass flow rate	kg/s
$\boldsymbol{\dot{m}_f}$	Fuel mass flow rate supplied to the combustor	kg/s
$\boldsymbol{\dot{m}_{f,reg}}$	Fuel mass flow rate for the regenerative cycle	kg/s
$\boldsymbol{\dot{m}_g}$	Total combustion-gas mass flow rate	kg/s
$\boldsymbol{\dot{m}_{g,reg}}$	Total combustion-gas mass flow rate for the regenerative cycle	kg/s
$\boldsymbol{\dot{m}_{CO_2}}$	Carbon dioxide mass emission rate	kg/s
$\boldsymbol{N}$	Number of ambient-temperature bins	—
$\boldsymbol{P}$	Absolute pressure at a thermodynamic state	kPa
$\boldsymbol{P_{amb}}$	Ambient atmospheric pressure	kPa

$P_{d,\text{reg}}$	Fractional pressure-loss coefficient of the regenerator	—
$\dot{Q}_{\text{in}}$	Combustor thermal energy input rate	kW
$\dot{Q}_{\text{in,reg}}$	Combustor thermal energy input rate for the regenerative cycle	kW
Q_{saved}	Recovered thermal energy rate	kW
r_p	Compressor pressure ratio	—
R_{air}	Specific gas constant for dry air	J/kg·K
s	Specific entropy	kJ/kg·K
SFC	Specific fuel consumption	kg/kWh
T	Absolute thermodynamic temperature	K
T_a	Ambient air temperature	°C or K
T_f	Fuel delivery temperature	K
TIT	Turbine inlet temperature	°C
$\dot{V}$	Compressor inlet volumetric flow rate	m³/s
$Weight_i$	Normalized climatic weighting factor for temperature bin i	—
$\dot{W}_{\text{comp}}$	Compressor power consumption	kW
$\dot{W}_{\text{net}}$	Net cycle power output	kW
$\dot{W}_{\text{net,annual}}$	Annual net electrical work/output	kWh or MWh
$\dot{W}_{\text{net,reg}}$	Net cycle power output for the regenerative cycle	kW
$\dot{W}_{\text{turb}}$	Turbine power output	kW
$\dot{W}_{\text{turb,reg}}$	Turbine power output for the regenerative cycle	kW
$CO_{2,\text{annual,SGT}}$	Annual CO_2 emissions from the simple gas turbine	ton/year
$CO_{2,\text{annual,RGT}}$	Annual CO_2 emissions from the regenerative gas turbine	ton/year
$\Delta CO_{2,\text{annual}}$	Annual CO_2 emissions reduction	ton/year
$CO_{2,\text{reduction}}$	CO_2 reduction percentage	%
$\Delta Fuel_{\text{annual}}$	Annual fuel savings	ton/year
ε	Regenerator effectiveness	—
η_c	Compressor isentropic efficiency	—
η_{comb}	Combustion efficiency	—
η_t	Turbine isentropic efficiency	—
η_{th}	Thermal efficiency of the cycle	—
$\eta_{\text{th,reg}}$	Thermal efficiency of the regenerative cycle	—
$\eta_{\text{thermal,annual}}$	Annualized thermal efficiency	—
ϕ	Equivalence ratio	—
ϕ_{annual}	Annual weighted equivalence ratio	—
ρ	Fluid density	kg/m³

References

[1] International Energy Agency (IEA). *Electricity in Libya*. Paris: International Energy Agency. Available online: IEA country profile for Libya (accessed October 25, 2024). https://www.iea.org/countries/libya/electricity

[2] Hassan, H. S., & Kendall, C. C. G. (2014). Hydrocarbon provinces of Libya: A petroleum system study. In L. Marlow, C. C. G. Kendall, & L. A. Yose (Eds.), *Petroleum Systems of the Tethyan Region* (AAPG Memoir 106, pp. 101–141). American Association of Petroleum Geologists. https://doi.org/10.1306/13431855M1063608

[3] Hermans, M., Bruninx, K., & Delarue, E. (2018). Impact of CCGT start-up flexibility and cycling costs toward renewables integration. *IEEE Transactions on Sustainable Energy, 9*(3), 1468–1476. https://doi.org/10.1109/TSTE.2018.2791679

[4] Gülen, S. C. (2023). *Gas and Steam Turbine Power Plants: Applications in Sustainable Power*. Cambridge University Press. https://doi.org/10.1017/9781108943475

[5] Shen, Y., Sun, X., Ji, Q., & Zhang, D. (2023). Climate events matter in the global natural gas market. *Energy Economics, 125*, 106887. https://doi.org/10.1016/j.eneco.2023.106887

[6] Maruf, M. H., July, S. A., Rabbani, M., Sahrani, S., Hossain Lipu, M. S., Sarker, M. R., et al. (2023). Energy and exergy-based efficiency, sustainability and economic assessment towards improved energy management of a thermal power plant: A case study. *Sustainability, 15*(6), 5452. https://doi.org/10.3390/su15065452

[7] Ehtiwesh, S., Gabbasa, A., & Ehtiwesh, I. (2023). The potential of using the incorporation of concentrated solar power and gas turbines in the South of Libya. *International Journal of Thermodynamics, 26*(4), 1–10. https://doi.org/10.5541/ijot.1293271

[8] Jamróz, M., Piwowarski, M., Ziemiański, P., & Pawlak, G. (2021). Technical and economic analysis of the supercritical combined gas-steam cycle. *Energies, 14*(11), 2985. https://doi.org/10.3390/en14112985

[9] Omar, H., Kamel, A., & Alsanousi, M. (2017). Performance of regenerative gas turbine power plant. *Energy and Power Engineering, 9*(2), 136–146. https://doi.org/10.4236/epe.2017.92011

[10] Goodarzi, M. (2016). Comparative energy analysis on a new regenerative Brayton cycle. *Energy Conversion and Management, 120*, 25–31. https://doi.org/10.1016/j.enconman.2016.04.079

[11] Durmuşoğlu, Y., Üst, Y., & Kayadelen, H. K. (2017). Thermoeconomic optimization and performance analysis of a regenerative closed Brayton cycle with internal irreversibilities and pressure losses. *Iranian Journal of Science and Technology, Transactions of Mechanical Engineering, 41*(1), 61–70. https://doi.org/10.1007/s40997-016-0043-3

[12] Kakaras, E., Doukelis, A., & Karellas, S. (2004). Compressor intake-air cooling in gas turbine plants. *Energy, 29*(12–15), 2347–2358. https://doi.org/10.1016/j.energy.2004.03.043

[13] Rahman, M. M., Ibrahim, T. K., Kadirgama, K., Mamat, R., & Bakar, R. A. (2011). Influence of operation conditions and ambient temperature on performance of gas turbine power plant. *Advanced Materials Research, 189–193*, 3007–3013. https://doi.org/10.4028/www.scientific.net/AMR.189-193.3007

[14] Basrawi, F., Yamada, T., Nakanishi, K., & Naing, S. (2011). Effect of ambient temperature on the performance of micro gas turbine with cogeneration system in cold region. *Applied Thermal Engineering, 31*(6–7), 1058–1067. https://doi.org/10.1016/j.applthermaleng.2010.10.033

[15] Cohen, H., Rogers, G. F. C., Saravanamuttoo, H. I. H., Straznicky, P., & Nix, A. (2017). *Gas Turbine Theory* (7th ed.). Pearson. ISBN 978-1292093093.

[16] Çengel, Y. A., Boles, M. A., & Kanoğlu, M. (2023). *Thermodynamics: An Engineering Approach* (10th ed.). McGraw-Hill.

[17] Walsh, P. P., & Fletcher, P. (2004). *Gas Turbine Performance* (2nd ed.). Blackwell Science/Wiley. https://doi.org/10.1002/9780470774533

[18] Boyce, M. P. (2012). Advanced industrial gas turbines for power generation. In M. P. Boyce, *Combined Cycle Systems for Near-Zero Emission Power Generation* (pp. 44–102). Woodhead Publishing. https://doi.org/10.1533/9780857096180.44

[19] Lefebvre, A. H., & Ballal, D. R. (2010). *Gas Turbine Combustion: Alternative Fuels and Emissions* (3rd ed.). CRC Press.

[20] Boyce, M. P. (2012). *Gas Turbine Engineering Handbook* (4th ed.). Elsevier. ISBN 978-0-12-383842-1.

[21] Kurt, H., Recebli, Z., & Gedik, E. (2009). Performance analysis of open cycle

gas turbines. *International Journal of Energy Research, 33*(3), 285–294. https://doi.org/10.1002/er.1472

[22] Fernández, D. A. P., Foliaco, B., Padilla, R. V., Bula, A., & González-Quiroga, A. (2021). High ambient temperature effects on the performance of a gas turbine-based cogeneration system with supplementary fire in a tropical climate. *Case Studies in Thermal Engineering, 26*, 101206. https://doi.org/10.1016/j.csite.2021.101206

[23] Mohapatra, A. K., & Sanjay. (2015). Comparative analysis of inlet air cooling techniques integrated to cooled gas turbine plant. *Journal of the Energy Institute, 88*(3), 344–358. https://doi.org/10.1016/j.joei.2014.07.006

[24] Kim, D.-J., Moon, Y.-H., Choi, B.-S., Ryu, H.-S., & Nam, H.-K. (2017). Impact of a heavy-duty gas turbine operating under temperature control on system stability. *IEEE Transactions on Power Systems, 33*(4), 4543–4552. https://doi.org/10.1109/TPWRS.2017.2781239

[25] Moon, S. W., & Kim, T. S. (2020). Advanced gas turbine control logic using black box models for enhancing operational flexibility and stability. *Energies, 13*(21), 5703. https://doi.org/10.3390/en13215703

[26] Bassily, A. M. (2001). Effects of evaporative inlet and aftercooling on the recuperated gas turbine cycle. *Applied Thermal Engineering, 21*(18), 1875–1890. https://doi.org/10.1016/S1359-4311(01)00054-0

[27] Khaliq, A., & Choudhary, K. (2006). Thermodynamic performance assessment of an indirect intercooled reheat regenerative gas turbine cycle with inlet air cooling and evaporative aftercooling of the compressor discharge. *International Journal of Energy Research, 30*(15), 1295–1312. https://doi.org/10.1002/er.1221

[28] Carapellucci, R., & Giordano, L. (2021). Regenerative gas turbines and steam injection for repowering combined cycle power plants: Design and part-load performance. *Energy Conversion and Management, 227*, 113519. https://doi.org/10.1016/j.enconman.2020.113519

[29] Khan, M. N. (2020). Energy and exergy analyses of regenerative gas turbine air-bottoming combined cycle: Optimum performance. *Arabian Journal for Science and Engineering, 45*(7), 5895–5905. https://doi.org/10.1007/s13369-020-04600-9

[30] Memon, A. G., Harijan, K., Uqaili, M. A., & Memon, R. A. (2013). Thermo-

environmental and economic analysis of simple and regenerative gas turbine cycles with regression modeling and optimization. *Energy Conversion and Management, 76*, 852–864. https://doi.org/10.1016/j.enconman.2013.07.076

[31] Abed, S., Khir, T., & Ben Brahim, A. (2016). Thermodynamic and energy study of a regenerator in gas turbine cycle and optimization of performances. *International Journal of Energy Optimization and Engineering, 5*(2), 25–44. https://doi.org/10.4018/IJEOE.2016040102

[32] Azeez, A. A., & Ogbe, E. E. (2024). Gas turbine performance improvement through cycle modification. *International Journal of Research Publication and Reviews, 5*(5), 1812–1821. https://doi.org/10.55248/gengpi.5.0524.1133

[33] Ogbe, E. E., Ossia, C. V., Saturday, E., & Ezekwem, C. (2023). Effect of regenerative effectiveness on the performance of simple gas turbine. *Scientia Africana, 22*(3), 247–260. https://doi.org/10.4314/sa.v22i3.22

[34] Dellenback, P. A. (2006). A reassessment of the alternative regeneration cycle. *Journal of Engineering for Gas Turbines and Power, 128*(4), 783–790. https://doi.org/10.1115/1.2179079

[35] Jamil, M. A., Goraya, T. S., Rehman, A. U., Yaqoob, H., Ikhlaq, M., Shahzad, M. W., & Zubair, S. M. (2022). A comprehensive design and optimization of an offset strip-fin compact heat exchanger for energy recovery systems. *Energy Conversion and Management: X, 14*, 100191. https://doi.org/10.1016/j.ecmx.2022.100191

[36] Do Nascimento, C. A. R., Mariani, V. C., & dos Santos Coelho, L. (2020). Integrative numerical modeling and thermodynamic optimal design of counter-flow plate-fin heat exchanger applying neural networks. *International Journal of Heat and Mass Transfer, 159*, 120097. https://doi.org/10.1016/j.ijheatmasstransfer.2020.120097